Automotive Science and Engineering, Vol. 14, No. 1, (2024), 4295-4303

Iran University of Science and Technology

Automotive Science and Engineering

Journal Homepage: ase.iust.ac.ir

ISSN: 2008-9899

Flexible UV Photodetectors with Enhanced Sensitivity for Smart Vehicles: Utilizing ZnO Nanorods

Seied Isa Koranian [1]*, Mahdi Gholampour [1], Hamid Mazandarani [2]

[1] Physics Group, Faculty of Basic Science, Imam Ali University

[2] Physics Department, Iran University of Science and Technology, Tehran, Iran

ARTICLE INFO

Article history:
Received : 5 Dec 2023
Accepted: 21 Jan 2024
Published: 3 Feb 2024

Keywords:
smart vehicles
piezo-potential
UV photodetector
piezo-phototronic effect
ZnO nanorods

A B S T R A C T

Harnessing nanomaterials and the piezo-phototronic effect, we engineered a high-performance ultraviolet (UV) photodetector (PD), unveiling a new frontier in optoelectronics. This novel device seamlessly integrates zinc oxide nanorods (ZnO NRs) onto a flexible polyethylene terephthalate-indium tin oxide (PET-ITO) substrate through a straightforward and efficient hydrothermal process. This unique nanostructure design outshines its competitors, producing significantly higher current under UV illumination despite a comparable detection area. The plot thickens with the intriguing "piezo-phototronic effect," where applying pressure under UV light amplifies the current and overall device efficiency. This groundbreaking discovery paves the way for cutting-edge optoelectronic applications, where nanomaterials and the piezo-phototronic effect join forces to redefine performance.

1. Introduction

The ability to detect light within the ultraviolet-visible (UV-Vis) range is essential for diverse applications, including optical communication [1], flame detection [2], remote control [3], optoelectronic circuits [4], UV radiation detection for skin cancer prevention [5], and chemical gas sensing [6]. Furthermore, UV PDs have several applications in smart cars, including: a) sun glare detection: UV PDs can monitor the amount of UV radiation entering the cabin, detecting potential sun glare that could impair the driver's visibility. This information can trigger the automatic activation of the sun visor or the adjustment of the vehicle's interior lighting to reduce glare and enhance visibility, b) auto-dimming mirrors: UV PDs are used in auto-dimming mirrors to adjust the mirror's brightness based on the amount of headlight glare from oncoming vehicles. When the UV PDs senses intense UV light, it triggers the mirror to dim automatically, reducing the driver's exposure to dazzling headlights and improving nighttime visibility, c) advanced driver assistance systems (ADAS): UV PDs are being explored for use in ADAS features such as adaptive cruise control (ACC) and lane departure warning systems (LDW) [7, 8]. By detecting UV light from the vehicle's surroundings, these systems can enhance their performance by better understanding the environment and making more informed decisions [7, 8].

One-dimensional nanostructures, characterized by large surface-to-volume ratios and precisely engineered surfaces, have emerged as highly promising candidates for high-performance PDs due to their heightened sensitivity to light [9,10]. ZnO nanostructures exhibit characteristics of n-type semiconductors with a wide direct band gap of 3.34 eV and a notable exciton binding energy of 60 meV [11,12]. Flexible PDs have made noteworthy

*Corresponding Author: Seied Isa Koranian
Email Address: Seiedisa.koranian@gmail.com
https://doi.org/10.22068/ase.2024.662

[DOI: 10.22068/ase.2024.662]

advancements, overcoming the constraints of traditional optoelectronic concepts [13,14].

PET-ITO, renowned for its flexibility, high conductivity, cost-effectiveness, and resistance to external mechanical forces, is often employed as a substrate for flexible PDs [15]. Wurtzite semiconductors such as ZnO display anisotropic properties along the c-axis and perpendicular to it [15]. The crystal structure of ZnO comprises tetrahedrally coordinated Zn^{2+} cations and O^{2-} anions, generating a dipole moment under pressure [16]. The accumulation of these dipole moments within the crystal gives rise to a piezoelectric field along the strain direction, known as the piezo-potential [16].

The exploration of the interplay between semiconductors, photoexcitation, and piezoelectric properties has given rise to the field of piezo-phototronics, allowing for the manipulation of carrier generation, separation, transportation, and recombination processes at interfaces or junctions [16].

In this study, we fabricated flexible ZnO NRs-based PDs, to systematically and comprehensively investigate their piezo-phototronic effects. Remarkably, the ZnO NRs-based UV PD exhibited substantial enhancements in photocurrent and photoresponsivity UVA region. Moreover, the application of a compressive strain of -0.20% to the PD resulted in an increased photocurrent, demonstrating the capability of the piezo-phototronic effect to enhance PD performance.

2. Experimental

The vertically growth of ZnO nanorod arrays on PET-ITO substrate involves a sequential two-step process:

a) Coating of ZnO seed layer on the substrate:

A seed layer was produced on a 1.5×1.5 cm^2 flexible PET-ITO substrate using a sol-gel-based spin coating technique. To commence the process, the substrate underwent a thorough cleaning procedure to ensure a pristine surface. Subsequently, 1 M ZnO sol was synthesized by meticulously combining absolute ethanol, zinc acetate dehydrates and, triethylamine under continuous stirring at 50°C for 20 minutes, resulting in a clear and homogeneous ZnO solution. The sol was then applied to the substrate with a spin coater, spinning it at 3000 rpm for 30 seconds to uniformly deposit a thin seed layer. Finally, to eliminate the solvent and precursor, the substrate was dried at 70°C.

b) Growth of well-aligned ZnO NRs arrays:

The intricate process of fabricating vertically aligned ZnO NRs arrays unfolded through a carefully orchestrated hydrothermal synthesis. To initiate this transformative journey, a synergistic blend of zinc nitrate hexahydrate, deionized water, and hexamethylenetetramine was carefully prepared. Two aqueous solutions, each containing 0.01M of zinc nitrate and HMTA, were prepared separately. Both solutions were then vigorously stirred together using magnetic agitation for 30 minutes at room temperature. This thorough mixing ensured the formation of a uniform and homogeneous mixture. This carefully crafted precursor solution was then delicately transferred into a stainless-steel Teflon-lined autoclave, depicted in Figure 1a. The stage was now set for the transformative hydrothermal treatment. As the autoclave was heated to a balmy 90°C, the samples, now poised for their metamorphosis, were horizontally immersed in the solution. This transformative phase lasted for a meticulous 4 hours, allowing the zinc ions to react with the hexamethylenetetramine and H_2O, resulting in the formation of vertically aligned ZnO NRs. Following this transformative phase, the samples underwent a cleansing ritual, meticulously rinsed with DI water multiple times to effectively eliminate any lingering reactants or solution remnants. This thorough rinsing step ensured the removal of impurities and ensured the purity of the synthesized ZnO NRs. Finally, the rinsed samples were air-dried, completing their metamorphosis into towering ZnO NRs arrays. The production of ZnO NRs UV PDs entailed a meticulously coordinated procedure that transformed ZnO NR arrays into operational devices. The initial step involved depositing a 150 nm-thick thin film of ITO onto the ZnO NRs, as the n-type contact for the device, using a technique called RF magnetron sputtering. For the establishment of the complementary contact, silver ink was precisely administered onto the PET-ITO substrate, forming a conductive path. This precise lithographic step ensured the accurate alignment of the silver contacts with the ZnO NRs, thereby establishing the essential electrical connection for the device. Figure 1b presents a schematic illustration of the fabricated ZnO NRs-based UV PD.

[DOI: 10.22068/ase.2024.662]

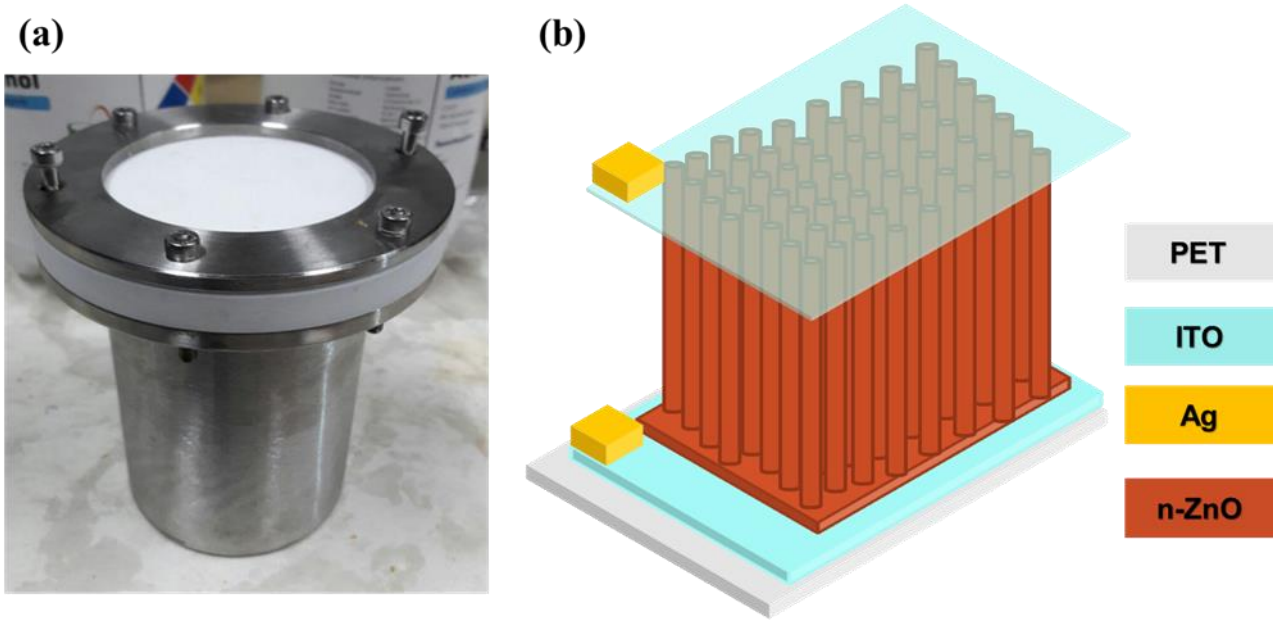

Figure 1: (a) stainless-steel Teflon-lined autoclave, (b) the schematic representation of the fabricated UV PD.

3. Result and discussion

3.1. Structural analysis

Figure 2a presents a top-view image obtained using scanning electron microscopy (SEM). It showcases the ZnO seed layer deposited on the PET-ITO substrate in impressive detail. The image reveals a densely packed and uniform layer, indicating successful preparation. The image reveals an average grain size of around 50 nm, showcasing the homogeneity and compactness of the seed layer.

Top-view SEM images of the well-aligned ZnO NRs grown on the flexible PET-ITO substrate with 100 and 20 nm magnitude are presented in Figure 2b and, Figure 2c, respectively. The SEM images highlight an exceptionally dense and uniformly spread network of ZnO NRs covering the entire surface of the PET-ITO substrate.

These NRs display a distinctive hexagonal morphology, with a diameter measuring approximately 40-50 nm, thereby providing additional confirmation of their successful growth. The cross-sectional SEM image depicted in Figure 2d validates the vertical growth of ZnO NRs on the substrate, exhibiting an average diameter of approximately 564 nm.

Figure 3a and, Figure 3b illustrates the X-ray diffraction (XRD) pattern of the ZnO seed layer and, the ZnO NRs, respectively. Indexing and comparison the XRD pattern with JCPDS cards (No. 36-1451 cards) and, (No. 75-1526) validate the wurtzite structure of the ZnO seed layer and ZnO NRs, respectively [12,17]. In Figure 3b, the increased intensity of the (002) reflection peak, along with the clear observation of (101) and (100) peaks, signifies a favored growth along the polar planes of the ZnO NRs, oriented perpendicular to the substrate [18,19]. This observation aligns with the SEM findings, providing additional support to this conclusion.

3.2. Optical analysis

UV-Vis spectra, depicted in Figure 4a, provide clues about the samples' optical properties, confirming their unique characteristics. Observing changes in these properties helps unravel the mechanisms governing electron transfer between the valence and conduction bands. The ZnO NRs exhibit a singular absorption peak centered around 356 nm [20]. A higher density of ZnO NRs enhances light exposure, maximizing the interaction of light with the underlying material. Furthermore, the perpendicular orientation of the nanorods, achieved through controlled vertical growth, significantly enhances light trapping compared to less vertically aligned nanorods.

[DOI: 10.22068/ase.2024.662]

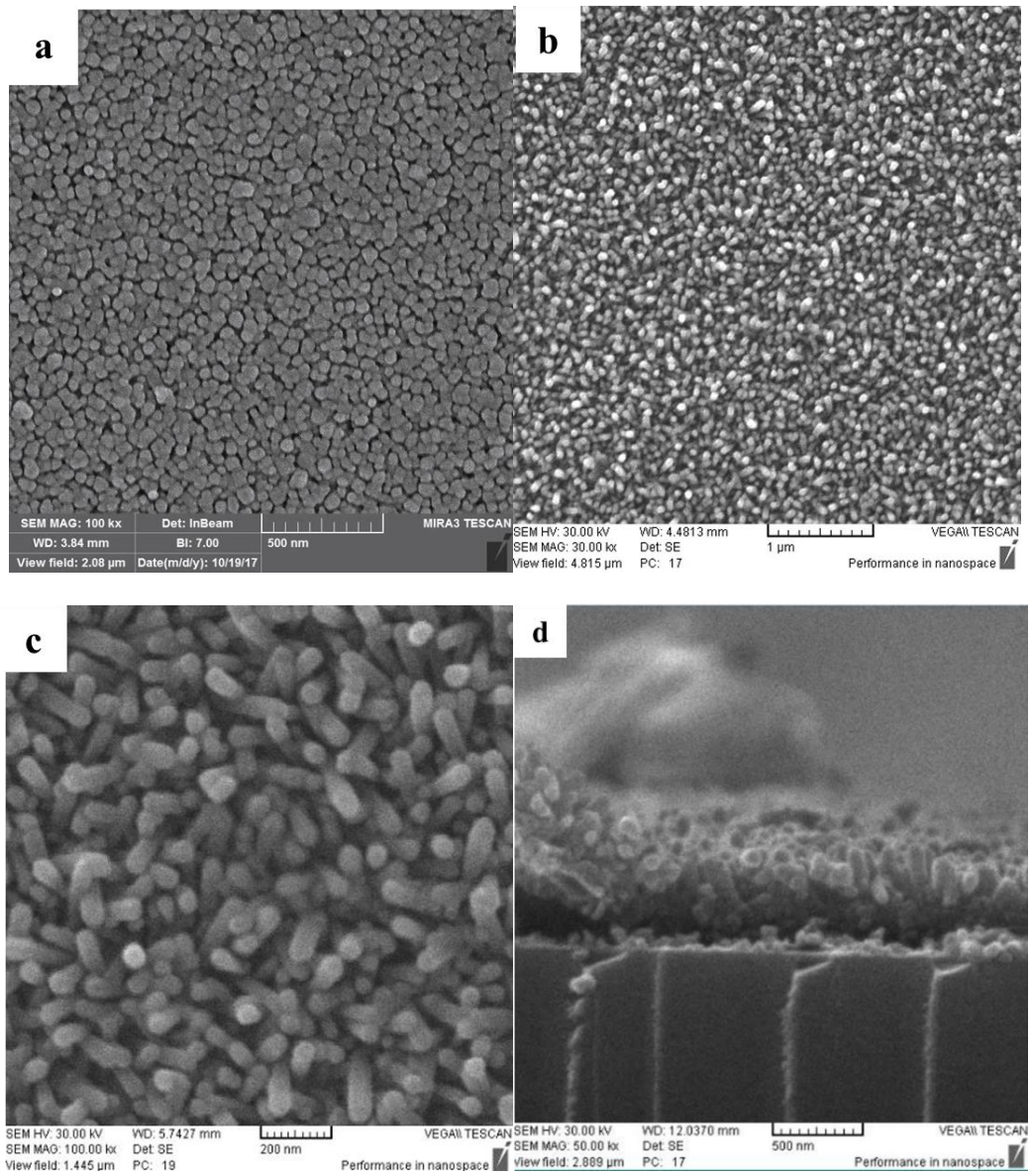

Figure 2: The top view SEM image of the (a) ZnO seed layer, and well-aligned ZnO NRs arrays with (b) 100 nm (c) 20 nm magnitudes. (d) cross-sectional SEM image of ZnO NRs

This is because the light travels a longer path within the nanorods, as schematically illustrated in Figure 4b. This efficient light trapping is crucial for maximizing the device's light absorption and overall performance [21]. In (1), a clear correlation is depicted between the light absorption (denoted as A) and optical path length traversing nanorods (denoted as x). Consequently, the increased optical path length in vertically aligned nanorods directly amplifies their capacity for light absorption [22].

$$A/I_0 = (1 - e^{\alpha x}) \quad (1)$$

Note that intensity of the incident light and the absorption coefficient denoted as I_0 and α, respectively. The transmission spectra of the prepared sample are shown in the inset of Figure 4a. According to the results, the prepared sample showed high transparency in the visible region.

The room-temperature photoluminescence (PL) spectra, as illustrated in Figure 5, reveal distinctive features for the ZnO NRs. Notably, there are dual emission peaks, one in the UV region (indicating near-band-edge (NBE) emission and free exciton transitions) and another in the visible region (associated with deep-level defect (DLD) transitions) that dominate the spectrum [9,20].

[DOI: 10.22068/ase.2024.662]

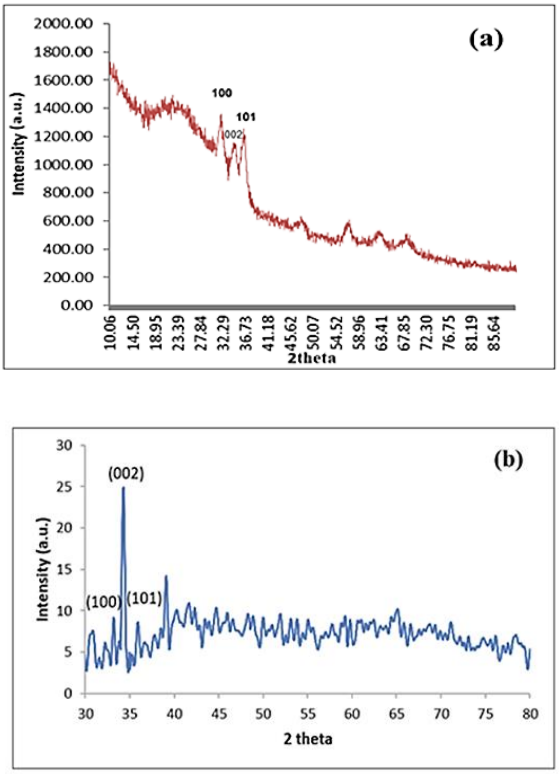

Figure 3: The XRD patterns of the (a) ZnO seed layer (b) well-aligned ZnO NRs arrays.

The strong dominance of UV emission over visible emission in the ZnO NRs, evident from the high ratio of their peak intensities, points towards minimal defects and superior crystal quality in the grown nanostructures [23].

3.3. Electrical characteristic

Figure 6 illustrate the current-voltage (I-V) characteristics of ZnO NRs under both dark and UV illumination conditions. Upon exposure to UV light, exhibit an increase in current at identical bias voltages. This phenomenon is ascribed to the photoexcitation of electrons in ZnO, prompting their transition from the valence band to the conduction band and the subsequent formation of free excitons [24]. The photocurrent can be determined using (2) [20]:

$$I_{\text{Photo current}} = I_{\text{Undr UV illumination}} - I_{\text{Dark condition}} \quad (2)$$

Where $I_{\text{Undr UV illumination}}$ is the current under UV illumination and $I_{\text{Dark condition}}$ is the current in dark condition. Figure 6 shows ZnO NRs PDs with photocurrents exceeding dark currents by ~3 orders of magnitude. Photoresponsivity (R), a measure of light sensitivity, is calculated using (3) [20]:

$$R(A/W) = I_{\text{Photo current}} / P_{\text{incident}} \quad (3)$$

Here the power of the incident light denoted as P_{incident}.

The notion of detectivity (D*), a fundamental measure assessing a photodetector's ability to distinguish subtle light signals amidst background noise, is quantifiable through (4) [25]:

$$D^* = \left(RA^{1/2}\right)/(2qI_{Dark\ condition})^{1/2} \quad (4)$$

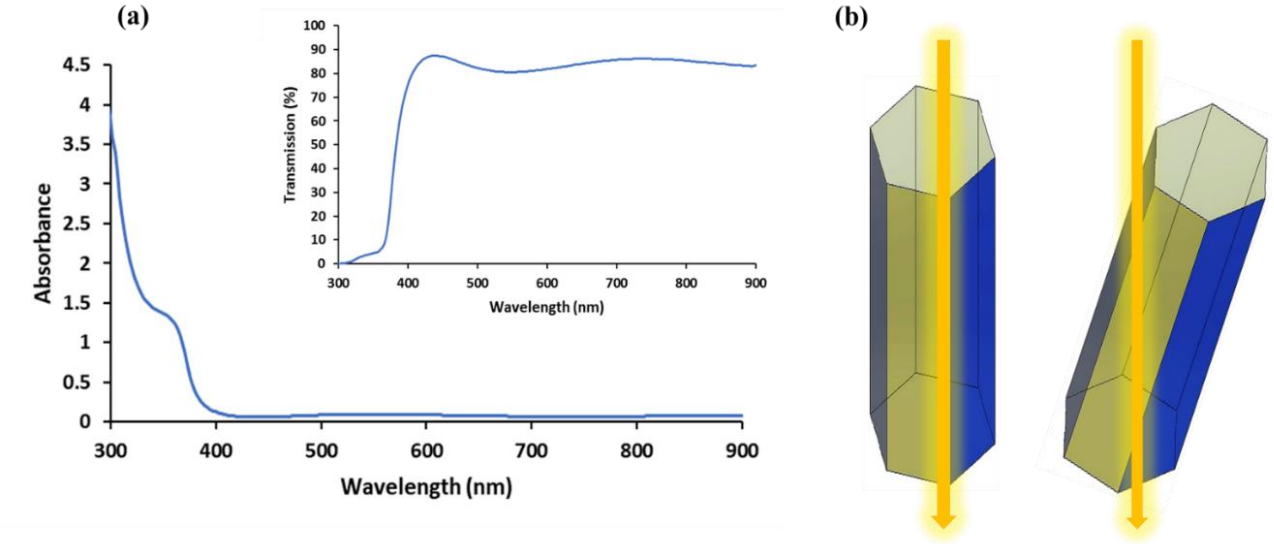

Figure 4: (a) Absorption spectra of the ZnO NRs. The inset shows the transmission spectra of the ZnO NRs. (b) the optical path traversing through nanorods

[DOI: 10.22068/ase.2024.662]

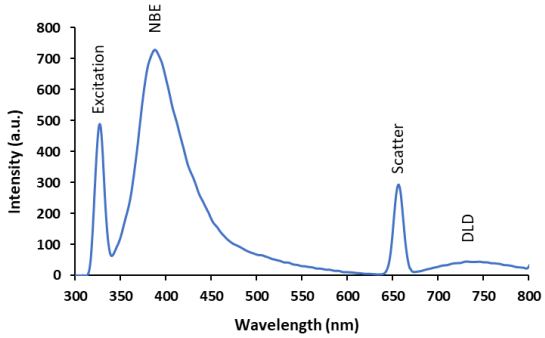

Figure 5: The room-temperature photoluminescence (PL) spectra of the ZnO nanorods

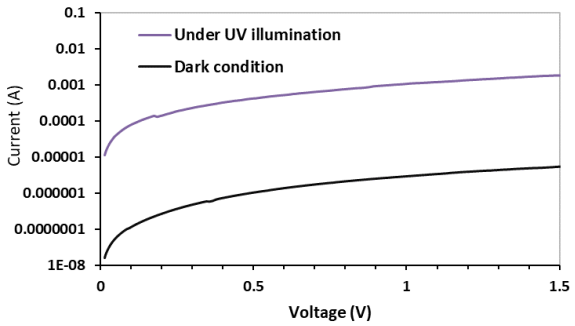

Figure 6: (a) I-V curves of the ZnO device under dark condition and UV illumination with 365 nm UV light

Table 1 summarizes the calculated values for key performance metrics of the device, including photocurrent, responsivity (R), and detectivity (D*).

Table 1. The specifications of fabricated PDs

Device	λ	Photo-current	Responsivity	Detectivity (Jones)
ZnO NRS	365 nm	0.43 mA	0.46 (A/W)	11×10^{10}

This research investigates the effects of externally applied different external strains (tensile and compressive form) on the transport of charge carriers in ZnO NRs-based UV PDs. This phenomenon, termed the piezo-phototronic effect, offers a novel avenue for manipulating the performance of these devices. A specifically designed setup, utilizing a stationary XYZ linear translation stage (Figure 7) allows for precise strain application, enabling a systematic analysis of its impact on the performance of the devices [26]. The strain values are determined using (5) [27]:

$$\text{Strain} = \frac{t_s+2r}{2R} \times 100 \quad (5)$$

Where t_s is the substrate thickness, r and R are the radius of the ZnO NRs, and the bending radius, respectively. A schematic depiction of the bending apparatus is presented in the inset of Figure 7 [27].

This methodology facilitates characterization and analysis of strain's impact on PD performance, elucidating the mechanisms and potential applications of the piezo-phototronic effect.

Figure 8 reveals the current-voltage (I-V) characteristics of the ZnO NRs PD under different levels of stress and UV illumination with 365 nm. This informative diagram sheds light on the device's performance and its response under varying strain and light conditions. Interestingly, the application of compressive strain enhances the photocurrent, increasing it from 0.43 mA to 0.54 mA within the -0.36% strain range. In contrast, tensile strain results in a decrease in photocurrent, dropping from 0.43 mA to 0.23 mA at a tension of 0.36%. These findings underscore a tangible correlation between strain and photo-response. Further insights are provided in Table 2, offering a comprehensive view of the device's performance through parameters such as responsivity, detectivity, and sensitivity.

Table 2 illustrates the significant impact of external forces on the photocurrent, responsivity, and detectivity of the device.

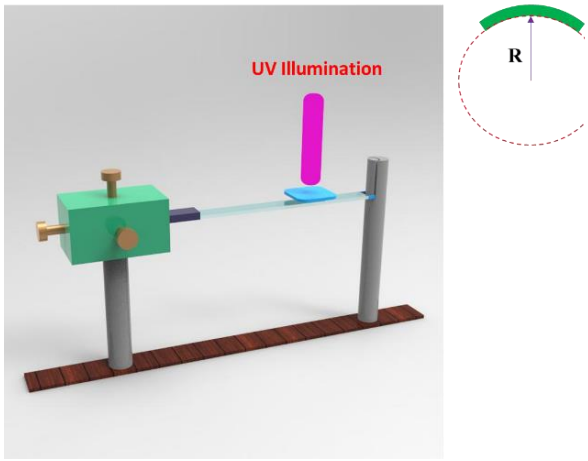

Figure 7: the experimental setup employed to generate compressive and tensile forces on the sample. The inset highlights the design of the bending apparatus.

[DOI: 10.22068/ase.2024.662]

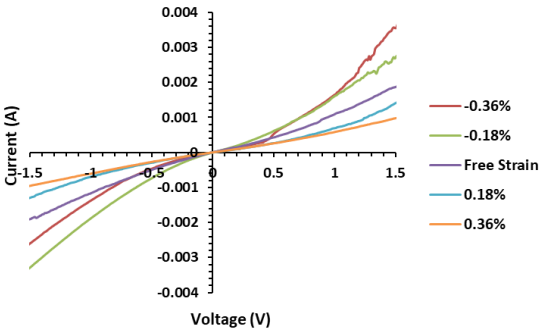

Figure 8: The I-V curves of the ZnO NRs-based PD were examined under UV illumination, with applied strains ranging from -0.36% to +0.36%

Table 2: The operational features of the manufactured ZnO nanorods-based photodetector were assessed under diverse strain conditions.

Sample	Photo-current	Responsivity	Detectivity (Jones)
-0.36%	0.54 mA	0.62 A/W	1.71×10^{10}
-0.18%	0.51 mA	0.58 A/W	1.49×10^{10}
Free strain	0.43 mA	0.46 A/W	1.18×10^{10}
0.18%	0.26 mA	0.29 A/W	0.74×10^{10}
0.36%	0.23 mA	0.25 A/W	0.65×10^{10}

The application of tensile or compressive strain induces the generation of negative or positive piezoelectric charges at the ZnO/ITO interface. These charges, in turn, modulate the barrier height at the junction, influencing the migrate of the photo-generated carriers. These findings underscore the robust correlation between external forces, the ensuing piezo-phototronic effect, and the performance parameters of the device [26]. The major contribution likely arises from the generation of piezo-charges at the interface between the ITO and ZnO, triggered by the applied strain [26]. During inward bending (compressive strain), negative piezo-charges arise at the ITO/ZnO interfaces. Equation (6) defines a quantitative correlation between the creation of negative piezo-charges and the consequent elevation in barrier height (BH), presumably driven by their impact on the interfacial potential profile [16].

$$\varphi_B = \varphi_{B0} - \frac{q^2 \rho_{piezo} W_{piezo}^2}{2\varepsilon_s} \quad (6)$$

In the given context, φ_B and, φ_{B0} represent the BH in the presence and absence of piezo-charges at the ZnO NRs /ITO interface, respectively. Here, q, ε_s, W_{piezo} and, ρ_{piezo} denotes the electric charge, the permittivity of the ZnO NRs, the width of the depletion layer in the presence of piezo-charges and, the polarization charge density, respectively. Squeezing the device (compressive strain) amplifies the built-in electric field within the material. This acts like a superhighway, efficiently separating and collecting the electron-hole pairs generated by light absorption [28, 29]. Additionally, the pressure induces negative charges at the interfaces, further widening the "depletion zone" where light absorption is most likely. This double whammy leads to more charge carriers reaching the electrodes, boosting the photocurrent (converted light into electricity) and overall light sensitivity [16]. On the other hand, stretching the device (tensile strain) has the opposite effect. Positive charges form at the interfaces, shrinking the depletion zone and weakening the electric field. This traffic jam hinders the separation and collection of charges, resulting in a weaker photocurrent and reduced light sensitivity [28, 29].

4. Conclusion

The primary aim of this investigation was to explore the impact of the piezo-phototronic effect on the performance of a UV PD utilizing ZnO NRs, cultivated on a PET-ITO substrate through hydrothermal deposition. Experiments demonstrated the developed photodetector's exceptional and consistent photoresponsivity, paving the way for its use in some application such as smart vehicles. Additionally, the study delved into the influence of the piezo-phototronic effect on the performance of the UV photodetector. Applying compressive and tensile strains emerged as an effective means to manipulate the transport properties of photo-generated electron-hole pairs, notably affecting their separation and recombination process. This finding opens exciting avenues for tailoring the performance of optoelectronic devices based on piezo-phototronic effects. Intriguingly, applying compressive strain led to a significant boost in photoresponsivity and overall PD performance. This finding highlights the potential of strain engineering for enhancing device performance, paving the way for the development of next-generation, high-efficiency UV PDs with improved flexibility and cost-effectiveness

[DOI: 10.22068/ase.2024.662]

5. References

[1] X. Deng, Z. Li, F. Cao, E. Hong, X. Fang, Woven fibrous photodetectors for scalable UV optical communication device, Adv. Funct. Mater. 33 (2023) 2213334.

[2] Q.-M. Fu, J.-L. Peng, Z.-C. Yao, H.-Y. Zhao, Z.-B. Ma, H. Tao, Y.-F. Tu, Y. Tian, D. Zhou, Y.-B. Han, Highly sensitive ultraviolet photodetectors based on ZnO/SnO2 core-shell nanorod arrays, Appl. Surf. Sci. 527 (2020) 146923. https://doi.org/https://doi.org/10.1016/j.apsusc.2020.146923.

[3] M. Xing, D. Jiang, M. Zhao, High external quantum efficiency in ZnO/Au/Ga2O3 sandwich–structured photodetector, Appl. Surf. Sci. 618 (2023) 156705. https://doi.org/https://doi.org/10.1016/j.apsusc.2023.156705.

[4] Y. Lin, J. Zou, W. Wang, X. Liu, J. Gao, Z. Lu, High-performance self-powered ultraviolet photodetector based on PEDOT:PSS/CuO/ZnO nanorod array sandwich structure, Appl. Surf. Sci. 599 (2022) 153956. https://doi.org/https://doi.org/10.1016/j.apsusc.2022.153956.

[5] M. Zheng, P. Gui, X. Wang, G. Zhang, J. Wan, H. Zhang, G. Fang, H. Wu, Q. Lin, C. Liu, ZnO ultraviolet photodetectors with an extremely high detectivity and short response time, Appl. Surf. Sci. 481 (2019) 437–442. https://doi.org/https://doi.org/10.1016/j.apsusc.2019.03.110.

[6] R.N. Gayen, R. Paul, S. Biswas, Schottky enabled enhanced UV detection by graphene oxide composited transparent ZnO thin films, Appl. Surf. Sci. 533 (2020) 147149. https://doi.org/https://doi.org/10.1016/j.apsusc.2020.147149.

[7] S. Royo, applied sciences An Overview of Lidar Imaging Systems for Autonomous Vehicles, 5 (2019). https://doi.org/10.3390/app9194093.

[8] X. Yu, M. Marinov, A Study on Recent Developments and Issues with Obstacle Detection Systems for Automated Vehicles, (2020).

[9] P. Gu, X. Zhu, D. Yang, Vertically aligned ZnO nanorods arrays grown by chemical bath deposition for ultraviolet photodetectors with high response performance, J. Alloys Compd. 815 (2020) 152346.

[10] M. Imamora, A. Umar, F. Yenni, N. Muhamad, M. Salleh, A. Ali, Hydrothermally grown of well-aligned ZnONRs : dependence of alignment ordering upon precursor concentration, J. Mater. Sci. Mater. Electron. 29 (2018) 6892–6897.

[11] A.S. Kamble, B.B. Sinha, K. Chung, M.G. Gil, V. Burungale, C.J. Park, J.H. Kim, P.S. Patil, Effect of hydroxide anion generating agents on growth and properties of ZnO nanorod arrays, Electrochim. Acta. 149 (2014) 386–393. https://doi.org/10.1016/j.electacta.2014.10.049.

[12] S. Pokai, P. Limnonthakul, M. Horprathum, P. Eiamchai, V. Pattantsetakul, S. Limwichean, N. Nuntawong, S. Porntheeraphat, C. Chitichotpanya, Influence of seed layer thickness on well-aligned ZnO nanorods via hydrothermal method, Mater. Today Proc. 4 (2017) 6336–6341.

[13] B. Liu, Z. Wang, Y. Dong, Y. Zhu, Y. Gong, S. Ran, Z. Liu, J. Xu, Z. Xie, D. Chen, G. Shen, ZnO-nanoparticle-assembled cloth for flexible photodetectors and recyclable photocatalysts, J. Mater. Chem. 22 (2012) 9379–9384. https://doi.org/10.1039/C2JM16781F.

[14] A. Manekkathodi, M.Y. Lu, C.W. Wang, L.J. Chen, Direct growth of aligned zinc oxide nanorods on paper substrates for low-cost flexible electronics, Adv. Mater. 22 (2010) 4059–4063. https://doi.org/10.1002/adma.201001289.

[15] D. Yang, Y. Qiu, Q. Jiang, Z. Guo, W. Song, J. Xu, Y. Zong, Q. Feng, X. Sun, Patterned growth of ZnO nanowires on flexible substrates for enhanced performance of flexible piezoelectric nanogenerators, Appl. Phys. Lett. 110 (2017). https://doi.org/10.1063/1.4975477.

[16] C. Pan, J. Zhai, Z.L. Wang, Piezotronics and Piezo-phototronics of Third Generation Semiconductor Nanowires, Chem. Rev. 119 (2019) 9303–9359. https://doi.org/10.1021/acs.chemrev.8b00599.

[17] T.H. Flemban, M.A. Haque, I. Ajia, N.

[DOI: 10.22068/ase.2024.662]

Alwadai, S. Mitra, T. Wu, I.S. Roqan, A Photodetector Based on p-Si/n-ZnO Nanotube Heterojunctions with High Ultraviolet Responsivity, ACS Appl. Mater. Interfaces. 9 (2017) 37120–37127.

[18] M.A. Khan, M.K. Singha, K.K. Nanda, S.B. Krupanidhi, Defect and strain modulated highly efficient ZnO UV detector: Temperature and low-pressure dependent studies, Appl. Surf. Sci. 505 (2020) 144365.

[19] A. GuruSampath Kumar, X. Li, Y. Du, Y. Geng, X. Hong, UV-photodetector based on heterostructured ZnO/(Ga,Ag)-co-doped ZnO nanorods by cost-effective two-step process, Appl. Surf. Sci. 509 (2020) 144770. https://doi.org/https://doi.org/10.1016/j.apsusc.2019.144770.

[20] M.A. Khan, M.K. Singha, K.K. Nanda, S.B. Krupanidhi, Defect and strain modulated highly efficient ZnO UV detector: Temperature and low-pressure dependent studies, Appl. Surf. Sci. 505 (2020) 144365. https://doi.org/10.1016/j.apsusc.2019.144365.

[21] J.R. Sharma, G. Das, A.B. Roy, S. Bose, S. Mukhopadhyay, Design Analysis of Heterojunction Solar Cells with Aligned AZO Nanorods Embedded in p-type Si wafer, Silicon. 12 (2020) 305–316.

[22] Y. Ren, Z. Yuan, J. Fan, W. Huang, C. Shuai, Annealing temperature-dependent morphology, structure, and optical properties of well-aligned ZnO nanowire arrays, Appl. Phys. A Mater. Sci. Process. 124 (2018) 0.

[23] J. Yang, J. Lang, C. Li, L. Yang, Q. Han, Y. Zhang, D. Wang, M. Gao, X. Liu, Effects of substrate on morphologies and photoluminescence properties of ZnO nanorods, Appl. Surf. Sci. 255 (2008) 2500–2503. https://doi.org/10.1016/j.apsusc.2008.07.124.

[24] S. Singh, Y. Kumar, H. Kumar, S. Vyas, C. Periasamy, P. Chakrabarti, S. Jit, S.H. Park, A study of hydrothermally grown ZnO nanorod-based metal-semiconductor-metal UV detectors on glass substrates, Nanomater.Nanotechnol. 7 (2017) 1–5. https:/doi.org/10.1177/1847980417702144

[25] H. Zhou, P. Gui, L. Yang, C. Ye, M. Xue, J. Mei, Z. Song, H. Wang, High performance, self-powered ultraviolet photodetector based on a ZnO nanoarrays/GaN structure with a CdS insert layer, New J. Chem. 41 (2017) 4901–4907.

[26] W. Peng, X. Wang, R. Yu, Y. Dai, H. Zou, A.C. Wang, Y. He, Z.L. Wang, Enhanced Performance of a Self-Powered Organic/Inorganic Photodetector by Pyro-Phototronic and Piezo-Phototronic Effects, Adv. Mater. 29 (2017) 1–9. https://doi.org/10.1002/adma.201606698.

[27] S.S. Kwon, W.K. Hong, G. Jo, J. Maeng, T.W. Kim, S. Song, T. Lee, Piezoelectric effect on the electronic transport characteristics of ZnO nanowire field-effect transistors on bent flexible substrates, Adv. Mater. 20 (2008) 4557–4562. https://doi.org/10.1002/adma.200800691.

[28] D. Jin, S. Ryong, G. Mohan, H. Dong, D. Young, P. Ilanchezhiyan, Applied Surface Science Piezo-phototronic effect triggered flexible UV photodetectors based on ZnO nanosheets / GaN nanorods arrays, Appl. Surf. Sci. 558 (2021) 149896. https://doi.org/10.1016/j.apsusc.2021.149896.

[29] S. Lee, R. Hinchet, Y. Lee, Y. Yang, Z.H. Lin, G. Ardila, L. Montès, M. Mouis, Z.L. Wang, Ultrathin nanogenerators as self-powered/active skin sensors for tracking eye ball motion, Adv. Funct. Mater. 24 (2014) 1163–1168. https://doi.org/10.1002/adfm.201301971.

[DOI: 10.22068/ase.2024.662]